Mutation Research 754 (2013) 39–50

Contents lists available at SciVerse ScienceDirect

Mutation Research/Genetic Toxicology and Environmental Mutagenesis

journal homepage: www.elsevier.com/locate/gentox
Community address: www.elsevier.com/locate/mutres

Genotoxicity of nano- and micron-sized manganese oxide in rats after acute oral treatment

Shailendra Pratap Singh[a], Monika Kumari[a], Srinivas I. Kumari[a], Mohammed F. Rahman[a], S.S. Kalyan Kamal[b], M. Mahboob[a], Paramjit Grover[a,*]

[a] Toxicology Unit, Biology Division, Indian Institute of Chemical Technology, Hyderabad, Andhra Pradesh 500 007, India
[b] Defence Metallurgical Research Laboratory, Kanchanbagh, Hyderabad, Andhra Pradesh 500 058, India

ARTICLE INFO

Article history:
Received 17 January 2013
Received in revised form 10 April 2013
Accepted 15 April 2013
Available online 22 April 2013

Keywords:
MnO_2-45 nm
MnO_2-bulk
Genotoxicity
Biochemical parameters
Biodistribution
Wistar rats

ABSTRACT

The use of nanotechnology has led to rapid growth in various areas. Manganese oxide (MnO_2) nanomaterials (NMs) are typically used for biomedical applications. However, characterizing the potential human health effects of MnO_2 NMs is required before fully exploiting these materials. The aim of this study was to investigate the acute oral toxicity of MnO_2 NMs and MnO_2-bulk particles in female albino Wistar rats. The genotoxic effects were examined using comet, micronucleus and chromosomal aberration assays. Nanosized MnO_2 (45 nm) significantly ($p < 0.01$) increased DNA damage in peripheral blood leukocytes and micronuclei and enhanced chromosomal aberrations in the bone marrow cells at 1000 mg/kg bw. These findings showed that the neurotoxicity of MnO_2-45 nm in the brain and red blood cells, as determined through acetylcholinesterase activity, was significantly ($p < 0.01$) inhibited at 1000 and 500 mg/kg bw doses. MnO_2-45 nm disrupted the physicochemical state and neurological system of the animals through alterations in ATPases *via* the total Na^+–K^+, Mg^{2+} and Ca^{2+} levels in the brain P_2 fraction. In addition, 500 and 1000 mg/kg bw doses of MnO_2-45 nm caused significant changes in AST, ALT and LDH levels in the liver, kidney and serum of treated rats. Significant tissue distribution was found in all tissues in a dose- and time-dependent manner. MnO_2-45 nm exhibited much higher absorptivity and tissue distribution compared with MnO_2-bulk. A large fraction of MnO_2-45 nm was cleared in the urine and feces. The histopathological analysis revealed that MnO_2-45 nm caused alterations in the liver, spleen and brain. These findings will provide fundamental information regarding the potential toxicities and biodistribution of nano and bulk MnO_2 generated through acute oral treatment.

1. Introduction

The advent of nanotechnology has led to the development of one of the major research fields of this century. During the last decade, nanotechnology has become an important part of this economy and has the potential to confer priceless advantages in different arenas such as medicine, aerospace, energy production and consumer products. Nanotechnology is quickly progressing, with approximately 1000 nanoproducts currently distributed in the market [1]. Nanomaterials (NMs) are particles with overall dimensions in the nanometer size range. The novel qualities of NMs have increased concerns regarding the potential for accidental effects on humans and the environment. Toxicology studies are therefore mandatory to address the potential adverse effects of NMs.

In the last 20 years a number of studies on the toxicology of NMs have been conducted. NMs, such as zinc oxide (ZnO), nickel oxide (NiO), titanium dioxide (TiO_2), gold (Au), silica, copper oxide (CuO) and silver (Ag), have shown an array of toxicological effects in a variety of *in vitro* and *in vivo* studies. MnO_2 NMs have been used as contrast agents for magnetic resonance imaging and drug delivery in medicine, as ionization-assisting reagents in mass spectroscopy, as biological agents in wastewater treatments and in consumer products, such as batteries [2–6]. The increased production and use of MnO_2 nanoparticles might increase the potential risk of toxicity through occupational exposure to humans and the environment. Therefore, the safety of MnO_2 NMs should be further investigated. Until recently, there has been a paucity of information concerning manganese oxide (MnO_2) NM toxicity. Many of the toxicity studies found in literature are *in vitro* or *in vivo* studies concerning the effects of other Mn oxide NMs on the respiratory system. The toxicity of insoluble Mn oxide NMs of various sizes and compositions was examined in ST-14 rat striated neuroblasts, using the MTT assay to evaluate mitochondrial function in living cells and the lactate dehydrogenase (LDH) assay to quantify the release of the enzyme LDH from damaged cell membranes. The results showed that the induction of oxidative stress and cell

* Corresponding author. Tel.: +91 40 27193135; fax: +91 40 27193227.
E-mail addresses: paramgrover@gmail.com, grover@iict.res.in (P. Grover).

1383-5718/$ – see front matter © 2013 Elsevier B.V. All rights reserved.
http://dx.doi.org/10.1016/j.mrgentox.2013.04.003

death occurred through apoptosis. Both assays revealed that Mn toxicity is dependent on the type and concentration of Mn oxide NMs used and the state of cell differentiation [7]. Mn nanoparticles exposed at 25–400 μg/ml activate mitochondrial-dependent apoptotic signaling and autophagy in N27 dopaminergic neuronal cells in a time- and dose-dependent manner and alter the expression of dopaminergic system-related genes in PC12 cells after exposure to 1 mg/ml Mn-40 nm [8,9]. Oxidative stress, cellular uptake and apoptosis were quantified in rat type II alveolar epithelial cells (AECs) exposed to Mn_3O_4 NMs. The production of reactive oxygen species (ROS) was observed in AECs treated with Mn_3O_4 NMs, which oxidized intracellular glutathione. Catalytic activity was also shown for Mn_3O_4 NMs. The increased uptake of manganese (Mn) in cells exposed to Mn_3O_4 NMs was detected in much higher amounts compared with that in cells exposed to Mn salt. Apoptosis was induced through both Mn_3O_4 NMs and Mn salt [10]. *In vitro* cytotoxicity was observed with MnO_2 nanoparticles using the live/dead cell assay, and LDH and ROS detection in various human cell lines, including lung adenocarcinoma, breast cancer cells and glioblastoma cells [11]. The toxicity of MnO_2 NMs was also evaluated in BRL 3A rat liver cells using a variety of *in vitro* assays. The results showed that higher doses (100–250 μg/ml) of MnO_2 resulted in LDH leakage [12]. The cellular morphology, mitochondrial function and dopamine concentration were assessed in a neuroendocrine cell line (PC-12) at 24 h after exposure to Mn NMs. The mitochondrial reduction activity and metal cytotoxicity were moderate for Mn-40 nm. Moreover, Mn NMs induced dose-dependent dopamine depletion [13]. The subacute intratracheal exposure of rats to MnO_2 led to a reduction in body weight. The relative weight of the lungs increased, and the weight of the liver was reduced in a dose- and time-dependent manner in the animals exposed to NMs. Mn was detected in the lungs and brain tissues, indicating that the NMs had crossed from the airways to the brain [14]. Intra-nasal and intratracheal subchronic application of MnO_2 NMs resulted in significant elevated Mn levels in the brain and blood and functional alterations in rats [15,16].

In vivo studies are essential to assess toxicants with adverse effects on human health. The *in vivo* study of NMs is of great importance because animal systems are extremely complicated, and the interaction of the nanostructures with biological components could lead to unique biodistribution, clearance, immune responses and metabolism [17]. The, gastrointestinal region is one of the most important portals of entry for NMs in humans and animals; hence, the oral route was used for the current study [18]. However, as far as we know the toxicity of MnO_2 NMs in rats through an oral route has not been performed. Therefore, we conducted an *in vivo* acute oral toxicity study of MnO_2 NMs and MnO_2-bulk particles in albino Wistar female rats. Histological assays are reliable tools to detect morphological changes due to toxicants; hence, the histopathology of various treated tissues was examined.

The systematic and ample characterization of NMs is important to understand the potential toxicity of these substances to biological systems [19]. In the present study, we determined the physicochemical properties of MnO_2-45 nm and MnO_2-bulk using transmission electron microscopy (TEM), dynamic light scattering (DLS), laser Doppler velocimetry (LDV) and surface area (Brunauer–Emmett–Teller) analyses.

Concerns about the risk of inducing cancer are universal, and as a result, genotoxicity studies are also essential to the safety assessment of chemicals. In the present study, the *in vivo* genotoxicity of MnO_2-45 nm and MnO_2-bulk particles was examined using the micronucleus test (MNT) and comet and chromosomal aberration (CA) assays. The comet assay is a sensitive method for the detection of DNA strand breaks and alkali-labile sites in individual cells induced through a variety of genotoxic agents [20]. MNT detects clastogenicity due to chromosome breakage, chromosome lagging and the dysfunction of mitotic apparatus. CAs result from failures in repair processes such that breaks either do not rejoin or rejoin in abnormal configurations.

Biochemical studies were also performed to assess conventionally used biomarkers, including acetylcholinesterase (AChE), ATPases, alanine aminotransferase (ALT)/glutamate pyruvate transaminase (GPT) and aspartate aminotransferase (AST)/glutamate oxaloacetate transaminase (GOT) and LDH, in various organs of the treated rats. Understanding the biodistribution of NMs is essential for assessing the amount of nanoparticles that enter target tissues or sites and for determining the anatomic fate, clearance, and biological effects of these substances. Hence, the effects of the test compounds on biodistribution were analyzed in the whole blood, liver, kidney, heart, brain, spleen, lungs, urine and feces of rats using inductively coupled plasma-mass spectrometry (ICP-MS). In the present study, the doses used to evaluate the genotoxicity, biochemical effects and tissue distribution of MnO_2 NMs ranged from 100 mg/kg body weight (bw) to 1000 mg/kg bw. The lowest treatment dose was intended to reflect the level of potential human exposure. However, the highest doses were utilized to obtain toxicity through accidental exposure to large amounts of MnO_2 NMs. Moreover, in this study, the higher doses were used to obtain detectable amounts of Mn after distribution in the animal. Similar high doses have been used in other studies to assess the toxicological effects of ZnO_2 and TiO_2 using different routes [21,22].

2. Materials and methods

2.1. Nanoparticles and chemicals

MnO_2 nanopowder of <30 nm size and ≥98.1% purity, according to the manufacturer's report, was purchased from Mukherjee Industries, Kolkata, India. MnO_2-bulk material (CAS No. 1313-13-9) of <5 μm in size, and ≥99% purity, low melting point agarose (LMA), normal melting point agarose (NMA), ethylenediamino tetraacetic acid (EDTA) disodium salt, phosphate-buffered saline (Ca^{2+}, Mg^{2+} free; PBS), ouabain, ethylene glycol bis-(amino ethyl ether) tetra acetic acid (EGTA) and quinidine sulfate were purchased from Sigma Chemical Co., St. Louis, USA. Adenosine triphosphate (ATP) and tris hydrochloride were obtained from Hi-Media, India. Cyclophosphamide (CP), was purchased from Endoxan Asta, Asta Medica A.G., Germany, and dissolved in distilled water immediately prior to use.

2.2. Characterization

The NMs were characterized using TEM, DLS, and LDV to evaluate the material size, size distribution, state of dispersion, and zeta potential of the NMs in the solution. The specific surface area analysis was determined using the Brunauer–Emmett–Teller (BET) technique.

2.2.1. Transmission electron microscopy of MnO_2 nano and bulk particles

TEM images of MnO_2 NMs and bulk particles were obtained to assess the size and morphology using a TEM (JEOL, JEM-2100, Japan), with an accelerating voltage of 200 kV. The TEM was equipped with a plunge freezer and cryo transfer holder to fix specimens in the frozen state and fitted with a Gatan 2Kx2K CCD camera for acquiring high-resolution images. Materials were suspended in water (1 mg/ml), and one drop of suspension was placed on a carbon-coated copper TEM grid and evaporated at room temperature. The NMs were examined using "advanced microscopy techniques" software for the digital TEM camera calibrated for NM size measurements. For the size measurement, 100 particles were calculated from random fields of view and images showing the general morphology of the NMs.

2.2.2. Dynamic light scattering and laser Doppler velocimetry of MnO_2 nanomaterials in the solution

The size of the NMs and agglomerates were measured through DLS and LDV using a Malvern Zetasizer Nano-ZS. This device uses a 4-mW He–Ne 633-nm laser to analyze the samples and an electric field generator for the LDV measurements. A volume of 50 ppm of freshly prepared MnO_2 NMs suspension in Milli Q water was ultra sonicated using a probe sonicator (UPH 100, Germany) for 10 min at 90% amplitude. The high concentration of the suspension was further diluted and adjusted to a lower concentration to acquire enough counts per second. The prepared samples were transferred to a 1.5-ml square cuvette for DLS measurements, and 1 ml of the suspension was transferred to a Malvern Clear Zeta Potential cell for LDV measurement. The mean NM diameter was calculated using the same software program as utilized in the NM distributions, and the polydispersity index (PdI) was used to

measure the size ranges present in the solution. The PdI scale ranges from 0 to 1, with 0 corresponding to monodisperse and 1 corresponding to polydisperse.

2.2.3. Surface area analysis

The specific surface area (m^2/g) of the MnO_2-45 nm and MnO_2-bulk particles was measured through N_2adsorption–desorption analysis at 77 K using the Brunauer–Emmett–Teller (BET) method on a surface area analyzer Quadrusorb-SI V 5.06 instrument (M/S Quanta chrome Instruments Corporation, USA).

2.3. Animals

Female albino Wistar rats, aged 6–8 weeks and weighing 80–120 g, were obtained from the National Institute of Nutrition, Hyderabad, India. The animals were acclimatized for one week in groups of five in polypropylene cages. The animals were fed a commercial pellet diet, provided water *ad libitum* and maintained under standard conditions of humidity (55–65%), temperature (22 ± 3 °C) and light (12 h light/12 h dark cycles). The study was approved by the Institutional Animal Ethics Committee.

2.4. Acute oral toxicity

The acute oral toxicity of MnO_2-45 nm and MnO_2-bulk particles was assessed using methods in accordance with the Organization for Economic Cooperation and Development (OECD) guidelines known, as the "acute oral toxicity-fixed dose method" (OECD-420) [23]. A single rat was treated with an initial 5-mg/kg bw dose, according to the sighting study. If no mortality and symptoms were observed, then a second rat received a 50-mg/kg bw dose, followed by 300-mg/kg bw dose and a final dose of 2000 mg/kg bw in sequence. Because mortality and toxic symptoms were not observed at any dose level in the sighting study, five rats treated with a 2000-mg/kg bw dose level for MnO_2-45 nm and MnO_2-bulk particles were used in the present study. Various tissues were harvested for histopathological examinations.

2.5. Histopathological evaluation

Histopathological studies were conducted to assess the changes in the organs, *i.e.*, heart, liver, spleen, brain and kidney of NM, bulk particle- and control-treated animals. The formalin-fixed tissues were trimmed, embedded in paraffin, and sliced into 5-μm-thick sections. The sections were stained with H&E and examined under a light microscope.

2.6. Genotoxicity, biochemical and biodistribution studies

The rats were randomly divided into positive control (for the genotoxicity studies), control and experimental groups. The experimental groups were further divided into three subgroups based on the acute toxicity data. Three different dose levels of MnO_2-45 nm and MnO_2-bulk, (100, 500, and 1000 mg/kg bw), were used to assess genotoxicity, biochemical parameters and biodistribution. All groups contained five animals per test per sampling time. For the genotoxicity studies, the sampling times were 6, 18, 24, 48 and 72 h, and to examine the biochemical parameters, samples were obtained at 3 and 14 days. The tissues for the biodistribution studies were harvested after 6 h, 24 h, 48 h, 72 h and 14 days. The doses for the experimental groups were obtained after diluting various doses of MnO_2-45 nm and MnO_2-bulk in Milli Q water after sonication using a probe sonicator (UPH 100, Germany) for 10 min at 90% amplitude. The control groups were treated with 5 ml/kg bw of Milli Q water, and the experimental groups were treated with MnO_2-45 nm and MnO_2-bulk (100, 500, and 1000 mg/kg bw) through oral gavage. CP, a known mutagen, was used as the positive control at a dose of 40 mg/kg bw injected intraperitoneally (i.p.) in a 0.01 ml/kg bw volume. All rats received a single dose, and all treated rats were sacrificed through cervical dislocation at the indicated sampling times.

2.7. Comet assay

The alkaline comet assay was conducted for the assessment of DNA damage, according to the guidelines of Tice et al. [20], with slight modifications. Three slides were prepared for each experimental condition. The cell viability was determined using Trypan blue exclusion. The peripheral blood was collected at 6, 24, 48 and 72 h after the dosing. One hundred cells per rat (50 cells analyzed in each slide) were scored at 400× using a fluorescence microscope (Olympus-Japan) equipped with a blue (488 nm) excitation filter and yellow (515 nm) emission (barrier) filter. The DNA breakage was measured using a Comet Image Analysis System, version 6 (Kinetic Imaging Ltd, Nottingham, UK). The % tail DNA damage was used to evaluate the DNA damage.

2.8. Micronucleus test

The MNT was conducted according to the method of Schmid [24], using bone marrow cells extracted from the femurs. The study was performed at 24 and 48 h after treatment, according to OECD guideline 474 [25]. Three slides were generated for each animal, and the slides were microscopically analyzed at 1000× magnification. A total of 2000 polychromatic erythrocytes (PCEs) per animal were randomly selected from the three slides and scored for the presence of micronuclei (MN).

2.9. Chromosomal aberration assay

The CA analysis was performed after rinsing the bone marrow cells (femur and tibia) from the rats [26]. Three slides for each animal were generated using the flame-dried technique. The CAs were identified using the established criteria of OECD guideline 475 [27]. The analysis was performed at 18 and 24 h. Five hundred well spread metaphases were selected to assess the presence of CAs, and 1000 or more cells were examined at both sampling times to determine the mitotic index (MI).

2.10. Biochemical assays

Biochemical parameters including, AChE, ATPases, AST, ALT and LDH were examined in red blood cells (RBCs), serum and different tissues (brain, liver and kidney) as previously described [28].

2.11. Mn content analysis in tissues

For the biodistribution studies, the animals were placed in metabolic cages after treatment to collect the samples. The urine and feces samples were collected at 6 h, 24 h, 48 h, 72 h and 14 days after the dosing. Whole blood, liver, kidneys, heart, brain, spleen and lungs were collected at 6 h, 24 h, 48 h, 72 h and 14 days. The samples were pre-digested in nitric acid overnight, and heated at 80 °C for 10 h, followed by additional heating at 130–150 °C for 30 min. Subsequently, a volume of 0.5 ml of 70% perchloric acid was added, and the samples were again heated for 4 h and evaporated nearly to dryness. Following digestion, the samples were filtered, and 2% HNO_3 was added to a final volume of 25 ml for analysis. The Mn content in the samples was determined using ICP-MS.

2.12. Statistical analysis

The statistically significant changes were analyzed using one-way ANOVA. The results were expressed as the means ± standard deviation (S.D.). Multiple comparisons were performed using Dunnett's test. All calculations were performed using Graph Pad Instat 3 software for Windows. The statistical significance for all tests was set at $p < 0.05$.

3. Results

3.1. Particle characterization

The size and appearance of the MnO_2 NMs and bulk particles were determined through TEM images (Fig. 1A and B). The mean size distribution of MnO_2-NMs and MnO_2-bulk particles was 45 ± 17 nm and 2.74 ± 29 μm, respectively, and the particles showed a spherical morphology. The DLS value for the MnO_2 NMs size in the Milli Q water suspension was 334.4 nm. The DLS results showed larger values than the NM sizes measured using TEM, indicating that MnO_2-45 nm formed larger agglomerates in water suspension. The zeta potential and electrophoretic mobility measurements were −1.23 mV and 4.50 μ (μm cm/V/s), respectively, at pH 7.0. The DLS and LDV data were beyond the detection limit for the bulk material. The specific surface area of MnO_2-45 nm and MnO_2-bulk particles, as determined through BET analysis, was 50.73 and 7.95 (m^2/g), respectively (Table 1).

3.2. Animal observation, food consumption, body weight and organ weight

No adverse signs, symptoms and mortality were observed in the animals treated with MnO_2-45 nm and MnO_2-bulk. However, at high doses, MnO_2-45 nm treated rats showed dullness, irritation and moribund symptoms. Moreover, no significant changes were observed in food consumption, body weight and relative organ weight (liver, kidney, brain, heart and spleen) in animals receiving acute doses of either compound (Supplementary Fig. S1A–C). Because mortality was not observed in rats receiving acute doses of MnO_2-45 nm and MnO_2-bulk particles at 2000 mg/kg dose, the LD_{50} of these compounds was greater than 2000 mg/kg bw, ranking

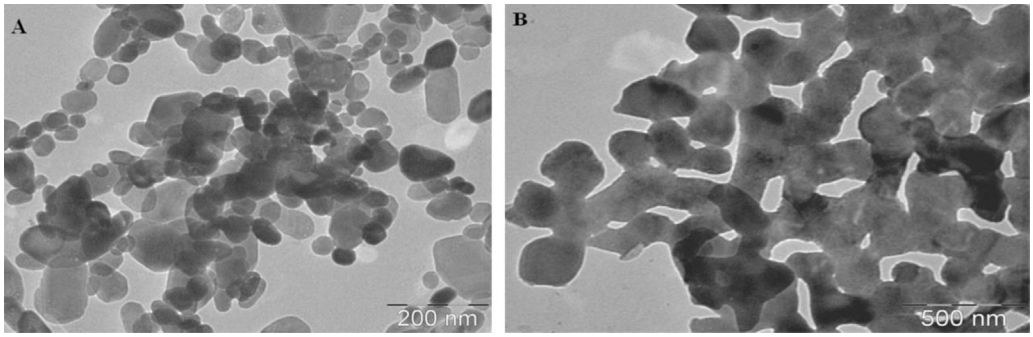

Fig. 1. Particle characterization of MnO_2-NMs (1A) and MnO_2-bulk (1B). MnO_2-NMs and MnO_2-bulk were dispersed in Milli Q water, mixing was done *via* probe sonication for 10 min.

Table 1
Particle characterization of MnO_2-NMs and MnO_2-bulk.

Nanomaterials	Size using TEM	DLS		LDV		pH	Surface area (m^2/g)
		Average diameter	PDI (nms)	Zeta potential ζ (mV)	Electrophoretic mobility μ (μm cm/V/s)		
MnO_2-NMs	45 ± 17 nm	330.4	0.576	−1.23	4.50	7.0	50.73
MnO_2-bulk	2.74 ± 29 μm	–		–	–	7.0	7.95

MnO_2-NMs and MnO_2-bulk were dispersed in Milli Q water, mixing was done *via* probe sonication for 10 min.

these substances into category 5, as per OECD guideline 420 [23] and the Globally Harmonized System (data not shown).

Supplementary material related to this article found, in the online version, at http://dx.doi.org/10.1016/j.mrgentox.2013.04.003.

3.3. Histopathological examinations

The spleen, brain and liver tissue of rats exposed to 2000 mg/mg bw of MnO_2 NMs through acute oral treatment revealed histopathological lesions; the spleen showed congestion, the brain depicted inflammation, and the liver displayed a dilated central vein (Fig. 2A–F). However, the tissues of rats exposed to 5, 50 and 300 mg/kg bw of MnO_2 NMs and 5, 50, 300 and 2000 mg/kg bw of MnO_2-bulk particles showed normal architecture of the spleen, brain, liver, heart and kidney tissues (data not shown).

3.4. Comet assay

The results obtained using the comet assay after acute oral treatment with MnO_2-45 nm and MnO_2-bulk particles are shown in Fig. 3A. In all samples, the cell viability, using the Trypan blue exclusion technique, was >90% (data not shown). A significant ($p < 0.05$) increase in the % tail DNA was observed in the peripheral blood leukocytes (PBLs) of rats exposed to MnO_2-45 nm at the highest dose of 1000 mg/kg bw at 24 and 48 h sampling times; however, no significant DNA damage was observed at 6 and 72 h. An increase in the % tail DNA was observed after treatment with lower doses of 100 mg/kg bw and 500 mg/kg bw in the MnO_2-45 nm treated groups, but these results were not statistically significant at all time intervals compared with the control groups. Significant DNA damage was not observed in rats treated orally with 100, 500 and 1000 mg/kg bw of MnO_2-bulk particles at 6, 24, 48, and 72 h. Moreover, CP significantly ($p < 0.01$) induced DNA damage in rat PBLs.

3.5. Micronucleus test

The results from the MNT are shown in Fig. 3B. The MNT data revealed and indicated statistically significant enhancement in the MN frequency in the groups treated with 1000 mg/kg bw of MnO_2-45 nm at 24 and 48 h of sampling times. At 24 h, the significance was $p < 0.05$, and at 48 h, the significance reached $p < 0.01$. However, treatment with 100 and 500 mg/kg bw of MnO_2-45 nm was not significant ($p > 0.05$) at both sampling times. Although the groups treated with MnO_2-bulk particles showed an increase in the frequency of MN-PCEs, this increase was not significant. However, CP induced a substantially significant ($p < 0.01$) effect on the frequency of MN-PCEs. The results of the MNT analysis with varied doses of MnO_2-45 nm and MnO_2-bulk materials did not reveal any statistically significant differences in % PCEs compared with the negative control at 24 and 48 h after treatment, demonstrating the absence of bone marrow cytotoxicity (Fig. 3C).

3.6. Chromosomal aberration assay

The results of the chromosomal aberration assay conducted after acute oral treatment with MnO_2-45 nm and MnO_2-bulk particles in bone-marrow cells of rats at 18 and 24 h are shown in Tables 2A and B, respectively. The effect of MnO_2-45 nm treatment on the induction of total cytogenetic changes was significant at the 1000 mg/kg bw dose (Tables 2A and B). In addition, treatment with NMs at 1000 mg/kg bw induced the same significant increases in the structural and numerical CAs and percentage of aberrant cells at the 18 and 24 h sampling periods. However, MnO_2-45 nm did not induce a significant increase ($p > 0.05$) in CA at 1000 and 500 mg/kg bw doses at both sampling times. Moreover, the MnO_2-bulk particles did not cause a significant increase ($p > 0.05$) in the total cytogenetic and structural (gaps, breaks, minute, acentric fragment and reciprocal translocation) changes, numerical (aneuploidy and polyploidy) CAs and percentage (%) of aberrant cells at all doses and treatment times. The MI did not reveal any significant differences ($p > 0.05$) between the various treatments at 1000, 500 and 100 mg/kg bw of MnO_2-45 nm and MnO_2-bulk particles compared with the control groups (Tables 2A and B).

3.7. Biochemical enzyme alterations

The acute oral treatment of rats with MnO_2-45 nm significantly inhibited RBC and brain AChE ($p < 0.01$) at 500 and 1000 mg/kg doses after 3 days and at the 1000 mg/kg dose after 14 days.

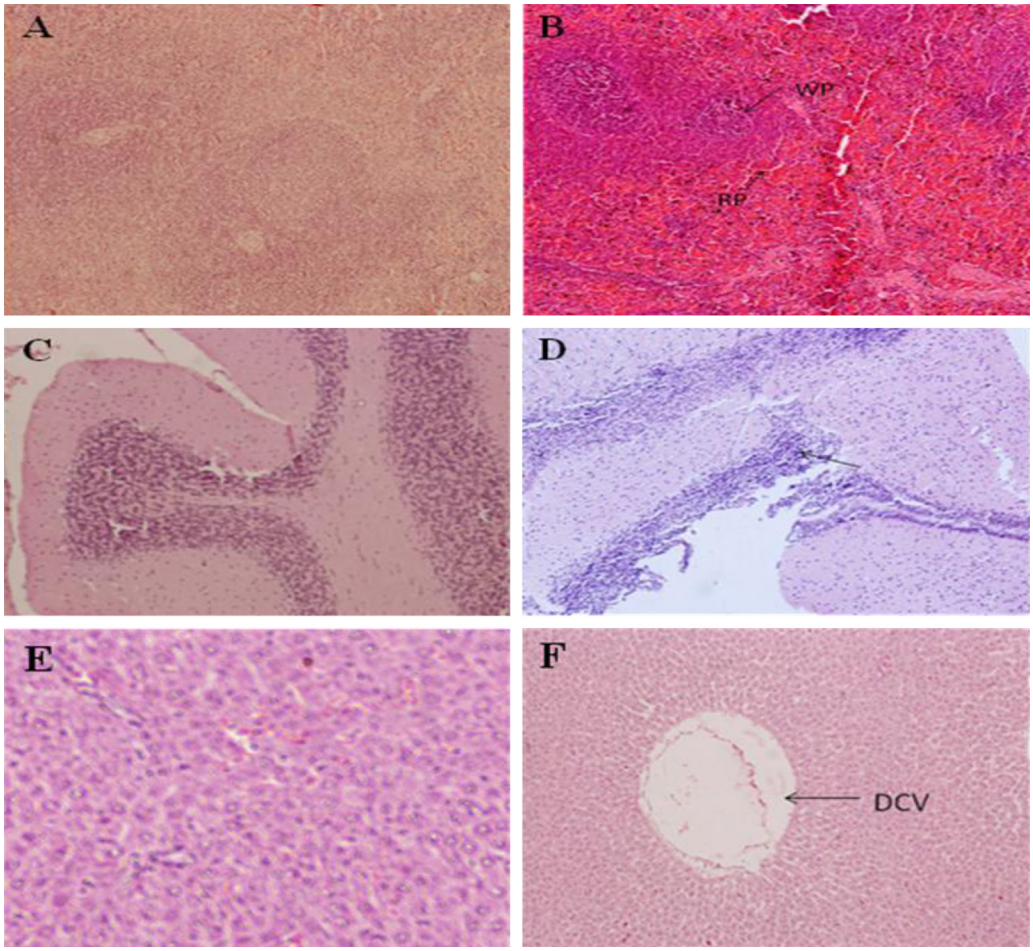

Fig. 2. Histopathology of spleen, brain and liver tissues of rats after acute oral treatment with MnO_2-45 nm. A, C and E showing the normal architecture of spleen, brain and kidney. B, D and F revealing the pathological alterations in spleen, brain and liver of MnO_2-45 nm (2000 mg/kg bw) treated group (indicated by arrow; magnification (100×).

Moreover, the brain AChE also showed a significant reduction at 100 mg/kg bw. Significant changes were not observed in RBC AChE levels in rats treated with MnO_2-bulk particles. However, MnO_2-bulk particles induced significant ($p < 0.05$) inhibition in brain AChE at a 1000 mg/kg dose after 3 days but not after 14 days of treatment (Fig. 4A and B).

Total, Na^+–K^+, $Mg^{2+}$and Ca^{2+}-ATPases were significantly ($p < 0.01$) inhibited at all three doses of MnO_2-45 nm in the brains of treated rats after 3 and 14 days. In addition, the observed changes were dose- and time-dependent. Similarly, rats exposed to the highest dose (1000 mg/kg bw) of MnO_2-bulk particles showed a significant ($p < 0.01$) decline in the total and Mg^{2+}-ATPases after 3 and 14 days (Fig. 4C–F).

The AST activity increased significantly with acute doses of MnO_2-45 nm in the serum and liver, but decreased in the kidney in a dose- and time-dependent manner. The alterations observed after MnO_2-bulk particle treatment were insignificant (Fig. 4G–I). The ALT activity increased in the serum and liver, whereas in the kidneys, ALT activity was reduced after treatment with MnO_2-45 nm. The ALT levels were significantly enhanced ($p < 0.01$) in the serum and liver at 500 and 1000 mg/kg doses after 3 days, and only after 14 days at 1000 mg/kg bw, whereas a significant reduction in the ALT activity was not observed in the kidneys at all doses of MnO_2-45 nm. Furthermore, exposure to MnO_2-bulk particles induced a significant ($p < 0.05$) increase in the ALT serum levels at the highest dose (1000 mg/kg bw) after 3 days (Fig. 4J–L).

The acute doses of MnO_2-45 nm induced an increase in the LDH activity in the serum, liver and kidneys. The serum LDH increased significantly at 500 and 1000 mg/kg bw doses at 3 and 14 days after MnO_2-45 nm exposure. There was a significant ($p < 0.01$) enhancement in the kidney LDH levels after acute oral treatment of MnO_2-45 nm at 1000 mg/kg bw after 3 and 14 days. The increase in the LDH levels was insignificant in the liver of rats treated with MnO_2-45 nm and in the serum, liver and kidneys of MnO_2-bulk-treated rats at all three doses (Fig. 4M–O).

3.8. Mn biodistribution

The biodistribution of Mn in the various organs, tissues, urine and feces of rats is shown in Fig. 5. Mn accumulated significantly in all of the tissues (whole blood, liver, heart, kidneys, brain and spleen) in animals treated with MnO_2-45 nm. After reaching the highest level at different time points in different organs, a gradual decrease in the Mn levels was observed in all of the organs. The maximum amount of Mn was detected in the liver, kidneys and blood at 24 h (Fig. 5A, B and F). In the brain, spleen, heart and lungs, the highest Mn level was detected at 48 h (Fig. 5C–E and G). The distribution of Mn at all time intervals was maximum after treatment with 1000 mg/kg bw of MnO_2-45 nm followed by 500 and 100 mg/kg bw MnO_2-45 nm treatments. However, a subsequent gradual decline in the Mn levels was observed in all tissues after 14 days. The MnO_2-bulk-treated groups did not show a statistically significant biodistribution of Mn in the kidneys, spleen, heart, blood, brain and urine compared with the control. Nevertheless, significant Mn accumulation in the liver was observed at 24 and 48 h after treatment with a dose of 1000 mg/kg bw (Fig. 5A). The

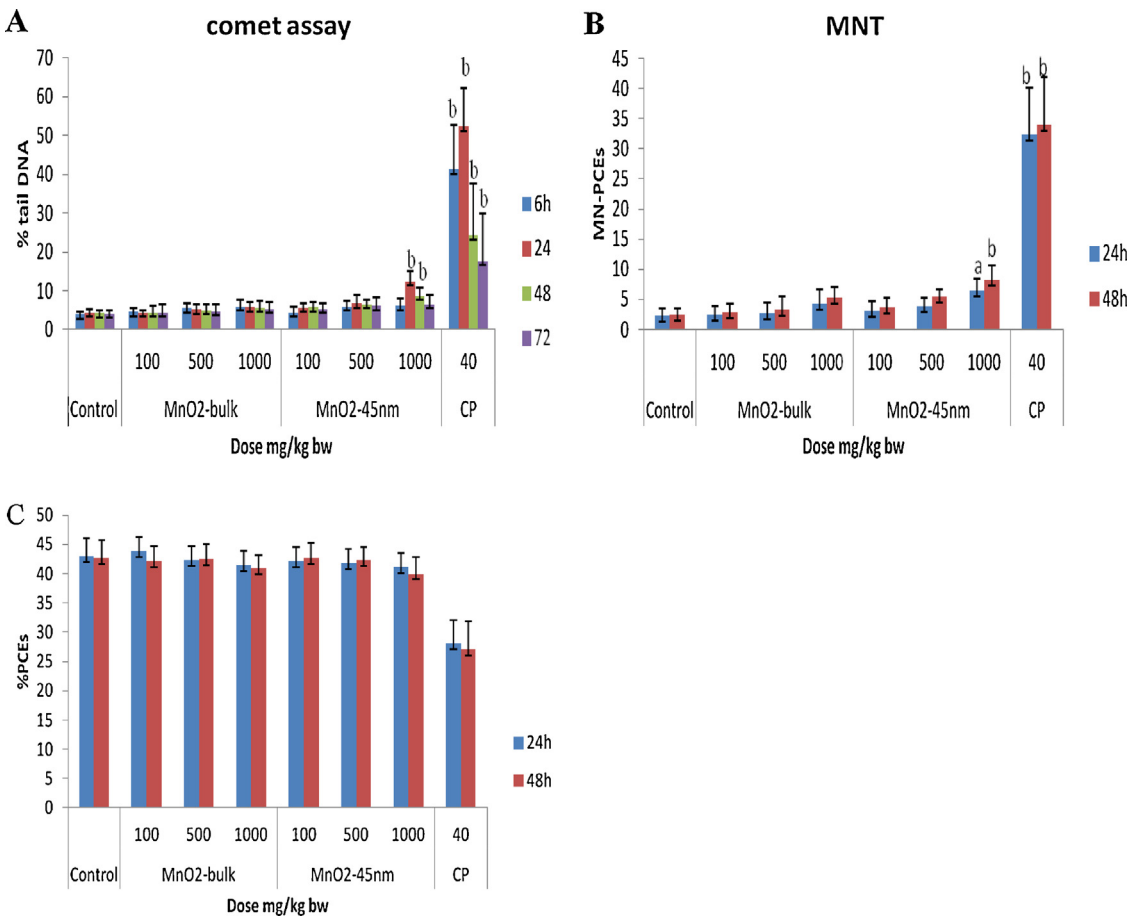

Fig. 3. The *in vivo* genotoxicity of MnO_2-45 nm and MnO_2-bulk particles. (A) Mean % tail DNA in peripheral blood leucocytes of female Wistar rats exposed orally to different doses of MnO_2-45 nm and MnO_2-bulk at 6, 24, 48 and 72 h. (B) Frequency of MN-PCEs and % PCEs in female Wistar rat bone marrow cells treated orally with different doses of MnO_2-45 nm and MnO_2-bulk at 24 h and 48 h. (C) Percentage PCEs observed in bone-marrow cells of female Wistar rats treated with different doses of MnO_2-45 nm and MnO_2-bulk at 18 h and 24 h. Deionised water (control), CP (cyclophosphamide, positive control), Data represented as mean ± S.D., significantly different from control at a = $p < 0.05$, b = $p < 0.01$, $n = 5$ animals per group.

absorption of Mn in various organs was high in the groups treated with NMs compared with the bulk particles-treated groups at all time points and dose levels. In the MnO_2-45 nm-treated rats, a significant amount of Mn was removed through the urine and feces (Fig. 5H). In contrast, MnO_2-bulk-treated rats showed large excretion in the feces (Fig. 5I). The clearance of Mn in the feces was rapidly reduced from 24 to 72 h. The excretion was highest after Mn treatment at with 1000 mg/kg bw dose, followed by treatment with 500 and 100 mg/kg bw doses. A significant increase in the Mn content was not observed in all of the tissues, urine and feces after 14 days in either the MnO_2-45 nm or the MnO_2-bulk-treated groups after acute oral treatment.

4. Discussion

There are numerous uses for nanotechnology in the everyday life of humans. However, because of the small size and large surface areas of these substances, NMs enter the human body *via* different routes, thereby posing an emerging threat to humans, the environment and food safety through the increasing use of NMs, although the toxicity of these compounds remains largely unexplored. The oral administration of 5, 50, 300 and 2000 mg/kg bw of MnO_2-45 nm and MnO_2-bulk in rats did not cause any obvious adverse effects in a 14-day acute toxicity study. However, the histopathological analysis of nano Mn-treated rats at a 2000 mg/kg bw dose showed inflammation in the brain, congested red and white pulp in the spleen and a dilated central vein in the liver. Similarly, ZnO-NMs showed hepatic swelling and vacuolization in the livers of the mice after acute oral administration [29]. The histopathological examination after acute oral and intraperitoneal treatment of mice with TiO_2-NMs revealed liver damage, pathological changes in the kidneys and lesions in the spleen [30,31].

The genotoxicity results obtained using the comet assay showed that MnO_2-45 nm induced significant % tail DNA in peripheral blood leukocytes after 24 and 48 h with the 1000 mg/kg bw dose and showed a steady time-dependent reduction in the % tail DNA. The observed gradual reduction in the % tail DNA might reflect modifications through complex DNA repair processes [32]. However, treatments with MnO_2-45 nm at 500 and 100 mg/kg bw doses and MnO_2-bulk particles at all three doses did not show a significant increase in the % tail DNA at all sampling times. Similar *in vivo* genotoxicity studies with MnO_2 NMs using the comet assay have not been reported.

The bone marrow MNT results revealed a significant increase in the MN frequency at 1000 mg/kg bw compared with the control, suggesting the genotoxicity of MnO_2-45 nm. However, variation in the MN frequency was observed at 24 and 48 h. Furthermore, the results of the MNT analysis indicated that low and medium doses of MnO_2-45 nm and all three doses of MnO_2-bulk particles were insignificant at both sampling times. The % PCEs calculated in the MnO_2-45 nm and MnO_2-bulk-treated groups did not show any significant reductions compared with the control group, suggesting

Table 2A
Chromosome aberrations and percent mitotic index observed in bone-marrow cells of female Wistar rats treated with different doses of MnO_2-45 nm and MnO_2-bulk at 18 h.

Dose (mg/kg bw)	M.I. (%) M ± SE	Chromosomal aberrations							Aberrant cells (%)	Total cytogenetic changes	TA + gaps M ± SE	TA − gaps M ± SE
		Numerical aberrations			Structural aberrations							
		Aneuploidy	Polyploidy	Gaps	Breaks	Minute	Acentric fragments	Reciprocal translocations				
Con.[A]	3.10 ± 0.51	0.8 ± 0.8	0.0 ± 0.0	0.6 ± 0.8	0.4 ± 0.5	0.2 ± 0.4	0.2 ± 0.6	0.00 ± 00	0.8 ± 0.44	2.4 ± 1.6	1.6 ± 1.1	1.0 ± 0.7
MnO_2-45 nm												
100	3.2 ± 0.20	1.2 ± 1.3	0.0 ± 0.0	1.0 ± 1.0	0.6 ± 0.5	0.4 ± 0.5	0.6 ± 0.6	0.0 ± 00	2.0 ± 1.0	3.8 ± 2.5	2.6 ± 1.5	1.6 ± 0.9
500	2.99 ± 0.23	1.4 ± 1.2	0.0 ± 0.0	1.4 ± 1.3	1.2 ± 1.0	1.0 ± 0.8	1.2 ± 0.8	0.0 ± 00	3.2 ± 1.7	6.0 ± 1.4	4.8 ± 1.6	3.4 ± 1.2
1000	3.05 ± 0.32	4.0 ± 1.0	0.0 ± 0.0	3.0 ± 2.0	1.8 ± 0.8	1.4 ± 1.0	1.6 ± 0.5	0.0 ± 00	7.0 ± 2.7[b]	11.8 ± 3.9[b]	7.8 ± 3.1	4.8 ± 1.3
MnO_2-bulk												
100	3.20 ± 0.44	1.2 ± 1.0	0.0 ± 0.0	0.8 ± 0.8	0.4 ± 0.5	0.4 ± 0.2	0.4 ± 0.5	0.0 ± 0.0	1.2 ± 0.83	3.2 ± 1.4	2.0 ± 1.8	1.2 ± 1.2
500	3.3 ± 0.37	1.0 ± 0.4	0.0 ± 0.0	1.0 ± 0.4	0.6 ± 0.4	0.6 ± 0.6	0.6 ± 0.8	0.0 ± 0.0	2.2 ± 1.4	3.8 ± 1.0	2.8 ± 1.7	1.8 ± 1.3
1000	3.11 ± 0.21	1.8 ± 1.0	0.0 ± 0.0	1.2 ± 0.8	1.0 ± 1.0	0.6 ± 0.5	1.2 ± 0.8	0.0 ± 0.0	2.6 ± 1.5	5.8 ± 2.5	4.0 ± 1.5	2.8 ± 1.7
CP[B]	1.83 ± 0.50	37.6 ± 4.5[b]	3.6 ± 1.2[b]	13.2 ± 3.1[b]	10.4 ± 2.7[b]	12 ± 3.1[b]	12.8 ± 3.2[b]	1.6 ± 0.9[b]	38 ± 2.9[b]	91.2 ± 14[b]	50 ± 9.8[b]	36.8 ± 7.5[b]

Significantly different from control at a = $p < 0.05$, b = $p < 0.01$. One hundred metaphases were analyzed per animal; $n = 5$ animals per group.
Total cytogenetic changes = numerical aberrations and structural aberrations. % Aberrant cells correspond to cells with ≥1 aberration excluding gaps. *Abbreviations*: MI, mitotic index; data represented as mean ± standard deviation; TA, total aberrations = structural aberrations.
[A] Negative control – deionised water.
[B] Cyclophosphamide (40 mg/kg bw).

Table 2B
Chromosome aberrations and percent mitotic index observed in bone-marrow cells of female Wistar rats treated with different doses of MnO_2-45 nm and MnO_2-bulk at 24 h.

Dose (mg/kg bw)	M.I. (%) M ± SE	Chromosomal aberrations							Aberrant cells (%)	Total cytogenetic changes	TA + gaps M ± SE	TA − gaps M ± SE
		Numerical aberrations			Structural aberrations							
		Aneuploidy	Polyploidy	Gaps	Breaks	Minute	Acentric Fragments	Reciprocal translocations				
Con.[A]	3.25 ± 0.30	0.6 ± 0.2	0.0 ± 0.0	0.8 ± 0.4	0.4 ± 0.4	0.4 ± 0.5	0.4 ± 0.5	0.00 ± 00	0.6 ± 0.54	2.6 ± 1.5	2.0 ± 0.8	1.2 ± 0.8
MnO_2-45 nm												
100	3.00 ± 0.53	1.2 ± 1.3	0.0 ± 0.0	0.8 ± 0.8	0.6 ± 0.9	0.6 ± 0.8	0.6 ± 0.4	0.00 ± 00	1.8 ± 0.45	3.8 ± 1.9	2.6 ± 0.9	1.8 ± 0.8
500	3.20 ± 0.44	1.8 ± 0.8	0.0 ± 0.0	1.4 ± 1.1	1.0 ± 0.8	0.6 ± 0.5	0.8 ± 0.8	0.00 ± 00	3.4 ± 1.1	5.6 ± 1.8	3.8 ± 1.3	2.4 ± 1.5
1000	3.04 ± 0.47	7.6 ± 2.9	0.0 ± 0.0	2.8 ± 2.0	2.0 ± 0.7	1.4 ± 0.5	2.0 ± 1.0	0.00 ± 00	7.4 ± 2.0[b]	15.8 ± 2.7[b]	8.2 ± 1.4[a]	5.4 ± 2[b]
MnO_2-bulk												
100	3.30 ± 0.32	1.2 ± 0.4	0.0 ± 0.0	1.0 ± 0.8	0.6 ± 0.5	0.4 ± 0.5	0.4 ± 0.4	0.0 ± 0.0	1.4 ± 0.6	3.6 ± 0.5	2.4 ± 0.8	1.4 ± 0.9
500	3.01 ± 0.63	1.4 ± 0.8	0.0 ± 0.0	1.2 ± 0.4	0.6 ± 0.8	0.6 ± 0.4	0.8 ± 1.0	0.0 ± 0.0	2.0 ± 0.5	4.6 ± 1.7	3.2 ± 1.0	2.0 ± 1.2
1000	3.15 ± 0.45	1.6 ± 1.0	0.0 ± 0.0	1.2 ± 1.0	0.8 ± 0.8	0.8 ± 0.4	1.0 ± 1.0	0.0 ± 0.0	2.4 ± 1.2	5.4 ± 2.3	3.8 ± 1.6	2.6 ± 1.5
CP[B]	1.90 ± 0.45	41.8 ± 4.7[b]	4 ± 2.1[b]	13 ± 3.16[b]	11 ± 2.7[b]	13.4 ± 2.8[b]	13.4 ± 1.3[b]	2 ± 1.0[b]	39 ± 4.3[b]	97.2 ± 12.5[b]	51.6 ± 11[b]	38.2 ± 4.8[b]

Significantly different from control at a = $p < 0.05$, b = $p < 0.01$. One hundred metaphases were analyzed per animal; $n = 5$ animals per group.
Total cytogenetic changes = numerical aberrations and structural aberrations. % Aberrant cells correspond to cells with ≥1 aberration excluding gaps. *Abbreviations*: MI, mitotic index; data represented as mean ± standard deviation; TA, total aberrations = structural aberrations.
[A] Negative control – deionised water.
[B] Cyclophosphamide (40 mg/kg bw).

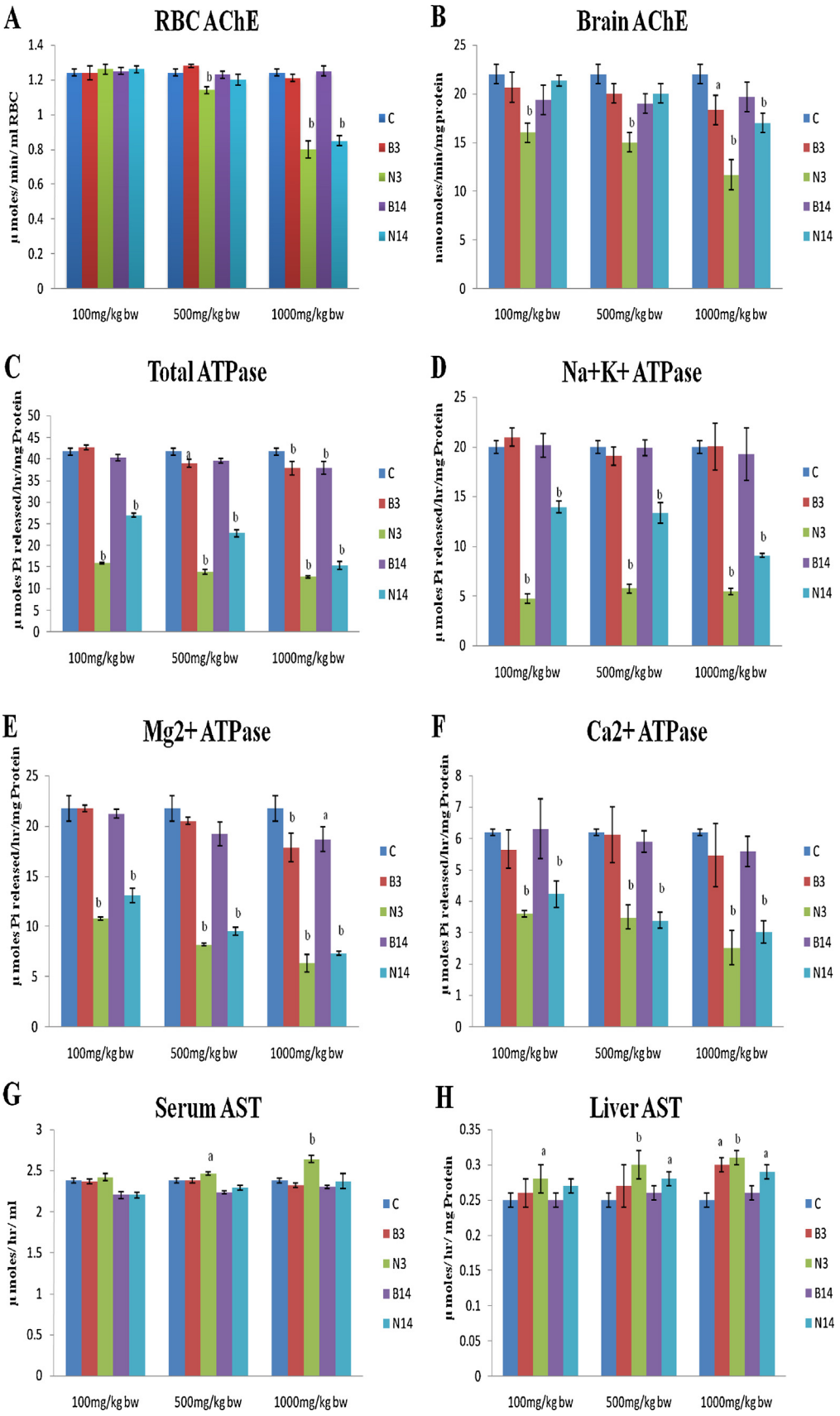

Fig. 4. Acute oral toxicity effect of MnO_2-45 nm and MnO_2-bulk on different enzymes in female albino Wistar rats. Data represented as mean ± S.D., significantly different from control at a, $p < 0.05$, b, $p < 0.01$, n, 5 animals per group (c). Compound and duration of oral treatments are abbreviated as MnO_2-bulk after 3rd day (B3), MnO_2-45 nm after 3rd day (N3), MnO_2-bulk after 14th day (B14), MnO_2-45 nm after 14th day (N14).

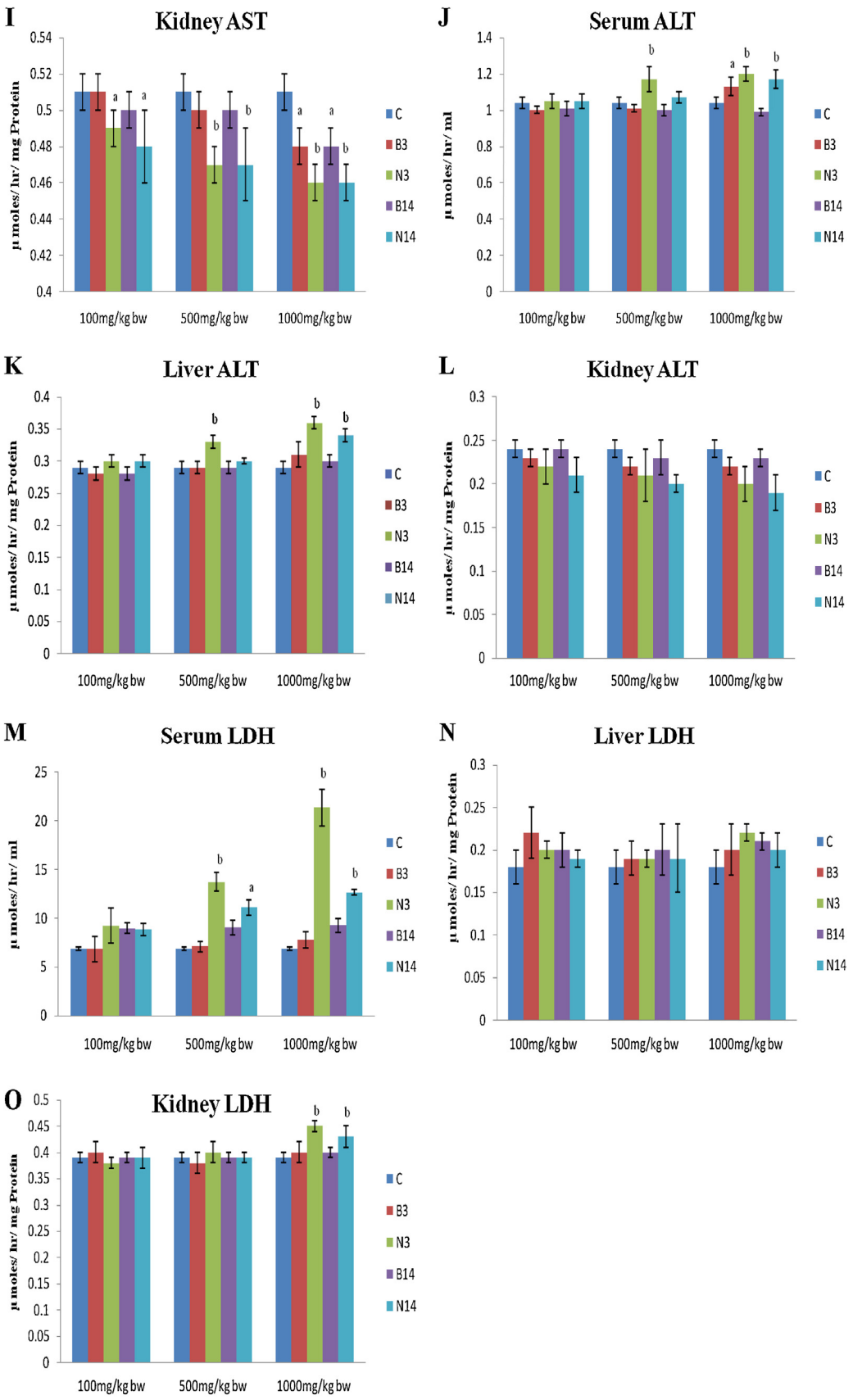

Fig. 4. (*Continued*)

that cell death had not occurred in any of the treated groups. These findings are consistent with an *in vivo* study in which TiO_2-NP, administered in drinking water for 5 days, induced a significant increase in the MN frequency in PCEs in mice [33].

The results of the CA analysis with MnO_2-45 nm and MnO_2-bulk in rats indicated that MnO_2-45 nm induces significant cytogenetic changes with the 1000 mg/kg bw dose, but not with the 500 and 100 mg/kg bw doses. However, MnO_2-bulk did not induce significant CA in bone marrow cells. The % MI suggested that MnO_2-45 nm and MnO_2-bulk were not cytotoxic.

The mechanism underlying the genotoxicity of NMs implicates oxidative stress, which causes a redox imbalance within cells as a result of increases in intracellular ROS. ROS generated in the metabolizing cells could attack the DNA base guanine and form 8-OHdG lesions, which have mutagenic potential [34]. An *in vitro* study in which PC-12 cells were exposed to Mn nanoparticles showed significant ROS generation (>10-fold), and a significant dose-dependent dopamine depletion was observed [13]. Similarly, when rat type II alveolar epithelial cells were exposed to Mn_3O_4 NMs, a significant increase in ROS generation and a dose-dependent increase in apoptotic cells were observed using the TUNEL assay [10]. Similarly, significant ROS were generated in the liver and brain mitochondria of rats treated intraperitoneally with manganese chloride ($MnCl_2$) at 15 and 30 mg/kg bw/day [35]. The genotoxicity observed in the MnO_2-45 nm-treated groups might potentially reflect increased ROS. Mn^{2+} generates both hydroxyl ($^{\bullet}OH$) and super-oxide ($^{\bullet}O_2^-$) radicals from H_2O_2 through the following equation: $Mn^{2+} + O_2 = Mn^{3+} + O_2^-$ and $Mn^{2+} + H_2O_2 = Mn^{3+} + OH^- + {}^{\bullet}OH$. The $^{\bullet}OH$ and $^{\bullet}O_2^-$ radicals attack DNA bases and ribose to form base adducts, such as 8-OHdG, or abstract hydrogen from C1 or C4 of ribose, resulting in single-strand breaks [36].

In the present study, MnO_2-45 nm exposure significantly inhibited RBC and brain AChE in dose- and time-dependent manner. The brain AChE activity was more affected, as even lower doses induced significant inhibition. However, the enzyme activity recovered with increasing treatment duration. Hence, after 14 days, the inhibition was less compared with that at 3 days. These results suggest the neurotoxicity of MnO_2 NMs. Furthermore, AChE could be a useful biomarker for NM-induced toxicity [37]. Consistent with the results obtained in the present study, rats administered with four or eight intraperitoneal injections of $MnCl_2$ at 25 mg/kg bw on alternate days showed a significant reduction in brain AChE activity at 24 h after the last injection [38].

The activities of total, Na^+–K^+, $Mg^{2+}$and Ca^{2+}-ATPases were significantly inhibited in a dose- and time-dependent manner in rat brains after exposure to MnO_2-45 nm, indicating that NMs might affect nerve conduction. In addition, higher doses of MnO_2-bulk particles also showed ATPase inhibition. Intraperitoneal exposure to Mn for 7 days did not affect Na^+–K^+-ATPase levels, while Mg^{2+}-ATPase was significantly activated [39]. These results suggest that the inhibition of Na^+–K^+-ATPase after Mn exposure might lead to neurotoxicity. Mn has been broadly reported as a neurotoxic agent in nanoform and bulk form (when extensively exposed) *in vitro* and *in vivo* [7,15,16,40].

In the present study, we showed that acute doses of MnO_2-45 nm significantly increased the activities of AST and ALT target enzymes in the serum and liver, whereas these enzymes were significantly reduced in the kidneys of the exposed rats in a dose- and time-dependent manner. The enhancement in the LDH levels in the serum, liver and kidneys after MnO_2-45 nm exposure was dose-dependent, revealing that there might be injuries in tissues in contrast to the observations in MnO_2-bulk and control-treated

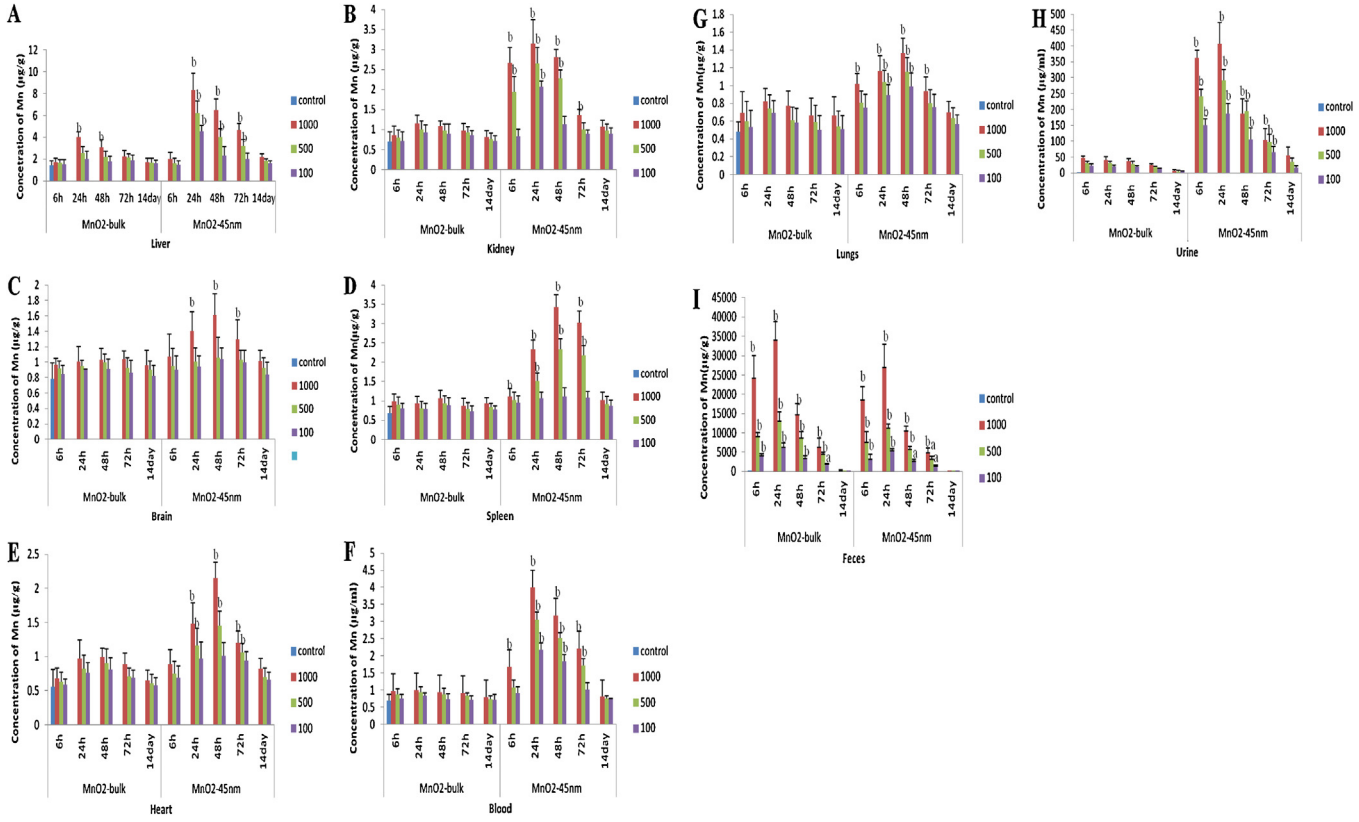

Fig. 5. Tissue distribution of Mn measured by ICP-MS in liver (A), kidney (B), brain (C), spleen (D), heart (E), blood (F), lungs (G), urine (H), feces (I) of rats after single oral administration of 1000 mg/kg, 500 mg/kg and 100 mg/kg bw of MnO_2-45 nm and MnO_2-bulk at 6, 24, 48, 72 h and 14 day of sampling time. Significantly different from control at a, $p < 0.05$, b, $p < 0.01$.

groups. The serum LDH levels increased in rats treated with higher doses of MNO_2-45 nm. Schrand et al. [41] reported that NMs interact with proteins and enzymes and interfere with the antioxidant defense mechanism, leading to ROS generation and subsequent apoptosis and necrosis.

Studies on the bioaccumulation of Mn after oral treatment with MnO_2-45 nm showed that the NMs were significantly distributed to organs, such as the liver, spleen, kidney, heart, blood, brain and lungs. The majority of NMs were detected in the liver, kidneys and spleen. The distribution pattern was dose- and time-dependent, as the amount absorbed increased with increasing dose administered. These finding suggests that MnO_2-45 nm crosses the gastrointestinal barrier and accumulates in the organs and tissues. The excretion data showed that a small quantity of NMs was excreted in the urine, whereas a large amount of NMs was excreted in the feces from 6–72 h. The tissue distribution of Mn with MnO_2-bulk-treated rats did not show a statistically significant increase in the kidneys, heart, spleen, lungs, blood, brain and urine at all of the time points and doses. However a significant increase was observed in the liver at 24 and 48 h in rats treated with MnO_2-bulk particles at a 1000 mg/kg bw. These results indicated that only a trace amount of MnO_2-bulk particles passes through the intestinal barrier and that a large amount of Mn is rapidly excreted in the feces at all of the time points. The Mn quantity was high in brains of the MnO_2-45 nm-treated groups compared with the MnO_2-bulk-treated groups. The results of the present study indicated that MnO_2 NMs penetrate the blood-brain barrier (BBB). Many studies have indicated that the divalent metal transporter-1 (DMT1) might be engaged in Mn influx into brain [42]. Mn binds to plasma transferrin (Tf). Hence, it has been suggested that the transport of the Mn–Tf complex into the brain relies on a transferrin receptor (TfR)-dependent mechanism, which competes with Fe transport or *vice versa*. However, recent studies have shown that the lack of functional DMT1 in knockout rats had no apparent effect on the brain influx of Mn ion or Mn–Tf [43].

Targeted NMs could be transported from circulating blood to the tissues of interest and could bind to molecular targets as a first step in nanoparticle retention or cellular internalization. Numerous NMs are rapidly cleared from the blood stream through the reticulo-endothelial-system (RES) and the mononuclear phagocytic system (MPS) in the liver, spleen and bone marrow [44,45]. The *in vivo* metabolic processes of Mn oxide NMs within the organism and the distribution of the substances in important organ tissues are not completely understood. A previous study with ultrafine manganese oxide particles in rats showed the translocation of Mn to the central nervous system. After twelve days of exposure, 3.5-fold increases were detected in the olfactory bulb and 2-fold increases were observed in the lungs. The liver concentration also increased after intranasal instillation [46]. Similarly, when Wistar rats were treated with MnO_2-NMs through intratracheal instillation for up to 9 weeks with 2.63 and 5.26 mg/kg bw doses, a statistically significant increase was observed in the Mn levels in the blood and brain [16]. Moreover, when rats were treated through sub-acute intratracheal instillation exposure with MnO_2-NMs for 3–9 weeks, Mn was detected in the lungs and brain samples of the groups treated with higher doses [14].

5. Conclusions

The results of the present study indicated a relatively low toxicity hazard in rats after the acute oral administration of nanoscale and bulk particle MnO_2. The results demonstrated that MnO_2-45 nm induces both genotoxicity and biochemical alterations. It is clear from these results that MnO_2-45 nm particles produce different results compared with MnO_2-bulk particles. According to these findings, exposure to MnO_2-45 nm and MnO_2-bulk particles at higher doses might induce neurotoxicity and liver and kidney damage. Although the underlying mechanism is not fully understood, oxidative stress and inflammation might be involved. Moreover, the NMs showed more bioaccumulation compared with the bulk materials. However, further studies are warranted for careful assessment to ensure the safety of MnO_2-NMs for occupational and general users. Hence, repeated dose and chronic studies are needed.

Conflict of interest

The authors declare that there are no conflicts of interest related to this research.

Acknowledgments

This work was financially supported through funding from the Department of Biotechnology, New Delhi, India (Grant No. BT/PR9998/NNT/28/84/2007). In addition, Shailendra Pratap Singh (SRF) received a fellowship from the Indian Council of Medical Research, India and Monika Kumari (SRF) received a fellowship from the University Grant Commission, India.

References

[1] S. Arora, J.M. Rajwade, K.M. Paknikar, Nanotoxicology and *in vitro* studies: the need of the hour, Toxicol. Appl. Pharmacol. 258 (2012) 151–165.
[2] H.B. Na, J.H. Lee, K. An, Y.I. Park, M. Park, I.S. Lee, D.H. Nam, S.T. Kim, S.H. Kim, S.W. Kim, K.H. Lim, K.S. Kim, S.O. Kim, T. Hyeon, Development of a T1 contrast agent for magnetic resonance imaging using MnO nanoparticles, Angew. Chem. Int. Ed. 46 (2007) 5397–5401.
[3] J. Shin, Md.A. Rahman, M.K. Ko, G.H. Im, J.H. Lee, I.S. Lee, Hollow manganese oxide nanoparticles as multifunctional agents for magnetic resonance imaging and drug delivery, Angew. Chem. Int. Ed. 48 (2009) 321–324.
[4] S. Taira, K. Kitajima, H. Katayangi, E. Ichiishi, Y. Ichiyanagi, Manganese oxide nanoparticle assisted laser desorption/ionization mass spectrometry for medical application, Sci. Technol. Adv. Mater. 10 (2009) 1–6.
[5] H. Chen, J. He, Facile synthesis of monodisperse manganese oxide nanostructures and their application in water treatment, J. Phys. Chem. C 112 (2008) 17540–17545.
[6] A. Rutz, Synthesis and properties of manganese oxide nanoparticles for environmental applications, in: The 2009 NNIN REU Research Accomplishments, 200998–99.
[7] D.M. Stefanescu, A. Khoshnan, P.H. Patterson, J.G. Hering, Neurotoxicity of manganese oxide nanomaterials, J. Nanopart. Res. 11 (2009) 1957–1969.
[8] H.A. Nagwa, A. Kanthasamy, Y. Gu, N. Fang, V. Anantharam, A.G. Kanthasamy, Manganese nanoparticle activates mitochondrial dependent apoptotic signaling and autophagy in dopaminergic neuronal cells, Toxicol. Appl. Pharmacol. 256 (2011) 227–240.
[9] J. Wang, M.F. Rahman, H.M. Duhart, G.D. Newport, T.A. Patterson, R.M. Murdock, Expression changes of dopaminergic system-related genes in PC12 cells induced by manganese, silver, or copper nanoparticles, Neurotoxicology 30 (2009) 926–933.
[10] R. Frick, B. Müller-Edenborn, A. Schlicker, B. Rothen-Rutishauser, D.O. Raemy, D. Günther, B. Hattendorf, W. Stark, B. Beck-Schimmer, Comparison of manganese oxide nanoparticles and manganese sulfate with regard to oxidative stress, uptake and apoptosis in alveolar epithelial cells, Toxicol. Lett. 205 (2011) 163–172.
[11] J.Y. Choi, S.H. Lee, H.B. Na, K. An, T. Hyeon, T.S. Seo, In vitro cytotoxicity screening of water-dispersible metal oxide nanoparticles in human cell lines, Bioprocess Biosyst. Eng. 33 (2010) 21–30.
[12] S.M. Hussain, K.L. Hess, J.M. Gearhart, K.T. Geiss, J.J. Schlager, In vitro toxicity of nanoparticles in BRL 3A rat liver cells, Toxicol. In Vitro 19 (2005) 975–983.
[13] S.M. Hussain, A.K. Javorina, A.M. Schrand, H.M. Duhart, S.F. Ali, J.J. Schlager, The interaction of manganese nanoparticles with PC-12 cells induces dopamine depletion, Toxicol. Sci. 92 (2006) 456–463.
[14] L. Sarkozi, E. Horvath, Z. Konya, I. Kiricsi, B. Szalay, T. Vezer, A. Papp, Subacute intratracheal exposure of rats to manganese nanoparticles: behavioral, electrophysiological, and general toxicological effects, Inhal. Toxicol. 21 (2009) 83–91.
[15] G. Oszlanczi, T. Vezer, L. Sarkozi, E. Horvath, A. Szabo, E. Horvath, Z. Konya, A. Papp, Metal deposition and functional neurotoxicity in rats after 3–6 weeks nasal exposure by two physicochemical forms of manganese, Ecotoxicol. Environ. Saf. 30 (2010) 121–126.
[16] G. Oszlanczi, T. Vezer, L. Sarkozi, E. Horvath, Z. Konya, A. Papp, functional neurotoxicity of Mn-containing nanoparticles in rats, Ecotoxicol. Environ. Saf. 73 (2010) 2004–2009.

[17] H.C. Fischer, W.C.W. Chan, Nanotoxicity: the growing need for in vivo study, Curr. Opin. Biotechnol. 18 (2007) 565–571.
[18] G. Oberdorster, E. Oberdorster, J. Oberdorster, Nanotoxicology: an emerging discipline evolving from studies of ultrafine particles, Environ. Health Perspect. 113 (2005) 823–839.
[19] R.C. Murdock, L. Braydich-Stolle, A.M. Schrand, J.J. Schlager, S.M. Hussain, Characterization of nanomaterial dispersion in solution prior to *in vitro* exposure using dynamic light scattering technique, Toxicol. Sci. 101 (2008) 239–253.
[20] R.R. Tice, E. Agurell, D. Anderson, B. Burlinson, A. Hartmann, H. Kobayashi, Y. Miyamae, E. Rojas, J.C. Ryu, Y.F. Sasaki, The single cell gel/comet assay: guidelines for in vitro and in vivo genetic toxicology testing, Environ. Mol. Mutagen. 35 (2000) 206–221.
[21] M. Baek, H.E. Chung, J. Yu, J.A. Lee, S.M. Paek, J.K. Lee, J. Jeong, J.H. Choy, S.J. Choi, Pharmacokinetics, tissue distribution, and excretion of zinc oxide nanoparticles, Int. J. Nanomed. 7 (2012) 3081–3097.
[22] T.H. Umbreit, S. Francke-Carroll, J.L. Weaver, T.J. Miller, P.L. Goering, N. Sadrieh, M.E. Stratmeyer, Tissue distribution and histopathological effects of titanium dioxide nanoparticles after intravenous or subcutaneous injection in mice, J. Appl. Toxicol. 32 (2012) 350–357.
[23] OECD Guidelines 420 Acute oral toxicity – fixed dose procedure (2001).
[24] W. Schmid, The micronucleus test, Mutat. Res. 31 (1975) 9–15.
[25] OECD Guidelines 474 genetic toxicology: micronucleus test (1997).
[26] I.D. Adler, Cytogenetic tests in mammals, in: S. Venitt, J. Parry (Eds.), Mutagenicity Testing: A Practical Approach, IRL Press, Oxford, 1984, pp. 273–306.
[27] OECD Guidelines 475 genetic toxicology: *in vivo* mammalian bone marrow cytogenetic test-chromosome analysis (1997).
[28] M. Kumari, S. Rajak, S.P. Singh, S.I. Kumari, P.U. Kumar, U.S.N. Murty, M. Mahboob, P. Grover, M.F. Rahman, Repeated oral dose toxicity of iron oxide nanoparticles: biochemical and histopathological alterations in different tissues of rats, J. Nanosci. Nanotechnol. 12 (2012) 2149–2159.
[29] C.H. Li, C.C. Shen, Y.W. Cheng, S.H. Huang, C.C. Wu, C.C. Kao, J.W. Liao, J.J. Kang, Organ biodistribution, clearance, and genotoxicity of orally administered zinc oxide nanoparticles in mice, Nanotoxicology 6 (2012) 746–756.
[30] J. Wang, G. Zhou, C. Chen, H. Yu, T. Wang, Y. Ma, G. Jia, Y. Gao, B. Li, J. Sun, Y. Li, F. Jiao, Y. Zhao, Z. Chai, Acute toxicity and biodistribution of different sized titanium dioxide particles in mice after oral administration, Toxicol. Lett. 168 (2007) 176–185.
[31] J. Chen, X. Dong, J. Zhao, G. Tang, In vivo acute toxicity of titanium dioxide nanoparticles to mice after intraperitioneal injection, J. Appl. Toxicol. 29 (2009) 330–337.
[32] A. Hartmann, G. Speit, Genotoxic effects of chemicals in the single cell gel (SCG) test with human blood cells in relation to the induction of sister-chromatid exchanges (SCE), Mutat. Res. 346 (1995) 49–56.
[33] B. Trouiller, R. Reliene, A. Westbrook, P. Solaimani, R.H. Schiestl, Titanium dioxide nanoparticles induce DNA damage and genetic instability in vivo in mice, Cancer Res. 15 (2009) 8784–8789.
[34] N. Singh, B. Manshian, G.J. Jenkins, S.M. Griffiths, P.M. Williams, T.G. Maffeis, C.J. Wright, S.H. Doak, NanoGenotoxicology: the DNA damaging potential of engineered nanomaterials, Biomaterials 30 (2009) 3891–3914.
[35] S. Zhang, Z. Zhou, J. Fu, Effect of manganese chloride exposure on liver and brain mitochondria function in rats, Environ. Res. 93 (2003) 149–157.
[36] G.B. Gerber, A. Leonard, P. Hantson, Carcinogenicity, mutagenicity and teratogenicity of manganese compounds, Crit. Rev. Oncol. Hematol. 42 (2002) 25–34.
[37] Z. Wang, J. Zhao, F. Li, D. Gao, B. Xing, Adsorption and inhibition of acetylcholinestrase by different nanoparticles, Chemosphere 77 (2009) 67–73.
[38] D. Santos, D. Milatovic, V. Andrade, M.C. Batoreu, M. Aschner, A.P.M. dos Santos, The inhibitory effect of manganese on acetylcholinestrase activity enhances oxidative stress and neuroinflammation in the rat brain, Toxicology 292 (2012) 90–98.
[39] C. Liapi, A. Zarros, P. Galanopoulou, S. Theocharis, N. Skandali, H. Al-Humadi, F. Anifantaki, E. Gkrouzman, Z. Mellios, S. Tsakiris, Effects of short-term exposure manganese on the adult rat brain antioxidant status and the activities of acetylcholinesterase, (Na^+,K^+)-ATPase and Mg^{2+}-ATPase: modulation by L-cysteine, Basic Clin. Pharmacol. Toxicol. 103 (2008) 171–175.
[40] J.D. Schroeter, D.C. Dorman, M. Yoon, A. Nong, M.D. Taylor, M.E. Andersen, H.J. Clewell III, Application of multi-route physiologically based pharmacokinetic model for manganese to evaluate dose dependent neurological effects in monkeys, Toxicol. Sci. 129 (2012) 432–446.
[41] A.M. Schrand, M.F. Rahman, S.M. Hussain, J.J. Schlager, D.A. Smith, S.F. Ali, Metal based nanoparticles and their toxicity assessment, Wiley Interdiscip. Rev. Nanomed. Nanobiotechnol. 2 (2010) 544–568.
[42] M.E. Conrad, J.N. Umbreit, E.G. Moore, L.N. Hainsworth, M. Porubcin, M.J. Simovich, M.T. Nakada, K. Dolan, M.D. Garrick, Separate pathways for cellular uptake of ferric and ferrous iron, Am. J. Physiol. Gastrointest. Liver Physiol. 279 (2000) G767–G774.
[43] J.S. Crossgrove, R.A. Yokel, Manganese distribution across the blood-brain barrier III. The divalent metal transporter-1 is not the major mechanism mediating brain manganese uptake, Neurotoxicology 25 (2004) 451–460.
[44] D. Peer, J.M. Karp, S. Hong, O.C. Farokhzad, R. Margalit, R. Langer, Nanocarriers as an emerging platform for cancer therapy, Nat. Nanotechnol. 2 (2007) 751–760.
[45] M. Ferrari, Cancer nanotechnology: opportunities and challenges, Nat. Rev. Cancer 5 (2005) 161–171.
[46] A. Elder, R. Gelein, V. Silva, T. Feikert, L. Opanashuk, J. Carter, R. Potter, A. Maynard, Y. Ito, J. Finkelstein, G. Oberdörster, Translocation of inhaled ultrafine manganese oxide particles to the central nervous system, Environ. Health Perspect. 114 (2006) 1172–1178.